(A proposal to Jefferson Lab PAC49)

Double Spin Asymmetry in Wide-Angle Charged Pion Photoproduction

J. Annand, D. Hamilton, R. Marinaro, G. Penman, R. Montgomery (spokesperson)

SUPA School of Physics and Astronomy, University of Glasgow, Glasgow G12 8QQ, UK

X. Bai, G. Cates (spokesperson), K. Gnanvo, N. Liyanage, V. Nelyubin, H. Nguyen

University of Virginia, Charlottesville, VA 232904

S. Barcus, A. Camsonne, J.P. Chen, D. Gaskell, J.-O. Hansen, W. Henry, D. Flay, M. Jones, C. Keppel, D. Mack, S. Malace, D. Meekins, R. Michaels, D. Nguyen, B. Sawatzky, G. Smith, H. Szumila-Vance, A.S. Tadepalli (spokesperson), B. Wojtsekhowski (spokesperson-contact), S. Wood

Thomas Jefferson National Accelerator Facility, Newport News, VA 23606

P. Datta, E. Fuchey, A.J.R. Puckett, S. Seeds

University of Connecticut, Storrs, CT 06269

C. Ayerbe, H. Bhatt, D. Bhetuwal, B. Devkota, J. Dunne, D. Dutta, L. El-Fassi, A. Karki

Mississippi State University, Mississippi State, MS 39762

V. Bellini, C. Sutera, V. Brio, F. Tortorici

Istituto Nazionale di Fisica Nucleare, I-95123 Catania, Italy

E. Cisbani, F. Meddi, G.M. Urciuoli

Istituto Nazionale di Fisica Nucleare - Sezione di Roma, P.le Aldo Moro, 2 - 00185 Roma, Italy

J.C. Cornejo, B. Quinn

Carnegie Mellon University, Pittsburgh, PA 15213

R. Gilman

Rutgers, The State University of New Jersey, New Brunswick, NJ 08854

F. Hauenstein

Old Dominion University, Norfolk, VA 23529
Massachusetts Institute of Technology, Cambridge, Massachusetts 02139, US

P. Markowitz

Florida International University, Miami, FL 33199

P. Monaghan

Christopher Newport University, Newport News, VA 23606

A. Sarty

Saint Mary's University, Halifax, Nova Scotia B3H 3C3, Canada

A. Schmidt

The George Washington University, Washington, DC 20052, USA

A. Shahinyan

AANL, 2 Alikhanian Brothers Street, 0036, Yerevan, Armenia

J. Bernauer, E. Cline

Stony Brook University, Stony Brook, NY 11794, US
Riken BNL Research Center, Upton, NY 11973, US

T. Averett, M. Satnik

College of William and Mary, Williamsburg, VA 23185, US

W. Tireman

Northern Michigan University, Marquette, Michigan 49855, US

M.E. Christy, T. Gautam

Hampton University, Hampton, Virginia 23669, USA

May 24, 2021

Contents

1 Executive Summary

1.1 Main physics goals

The goal for the pioneering measurement of the polarization transfer observable A_{LL} for single π^- photoproduction in the wide-angle regime is to address the following questions:

- What is the nature of the interaction mechanism of meson photoproduction from the nucleon at $s, -t, -u \gg \Lambda^2_{QCD}$?
- Does the twist-3 contribution dominate the twist-2 contribution in the wide angle regime, as suggested by the updated handbag mechanism cross section calculations?

We propose to measure A_{LL} for negatively charged pion photoproduction in the wide angle regime by using the SBS as the proton arm and BB as the pion arm. There, three aspects will be tested:

1. Does A_{LL} equal -K_{LL}?
2. Does A_{LL} have any dependence on cm. angle at $s = 9$ GeV^2 and large $-u$, $-t$?
3. Does A_{LL} have any s dependence at $s > 9$ GeV^2?

1.2 The proposed measurements/observables

This experiment will detect the pion and proton in single pion photoproduction from a neutron. Double polarization asymmetry will be obtained using a longitudinally polarized helium-3 target and longitudinally polarized electron beam. The time of data taking for these measurements are shown below.

E_{beam}	$< s >$	$< -t >$	$< -u >$	$\cos\theta_{CM}$	Beam on	Time	ΔA_{LL}
[GeV]	[(GeV/c)^2]	[(GeV/c)^2]	[(GeV/c)^2]		target [hour]	[hour]	accuracy
6.6	9.3	4.7	2.9	-0.23	6	37	$\pm$0.05
6.6	9.3	3.3	4.3	+0.14	8	27	$\pm$0.05
6.6	9.3	5.5	2.1	-0.44	8	27	$\pm$0.05
8.8	12.1	6.4	4.0	-0.23	16	47	$\pm$0.05
11.0	15.0	8.1	5.2	-0.23	60	98	$\pm$0.05

1.3 Specific requirements on detectors, targets, and beam

The experiment uses the detector packages of the BigBite and Super Bigbite Spectrometer for the luminosity of 4×10^{37} Hz/cm^2, which is about 10 times lower than in the GMn experiment E12-09-016. The polarized He-3 target with 60% polarization is the same as in the GEn/He-3 experiment. The experiment will use the 20 μA of 6.6, 8.8, and 11 GeV energy polarized CEBAF electron beam.

Abstract

We propose to measure the double spin asymmetry A_{LL} for charged pion photoproduction in the wide angle regime using the reaction ($\vec{\gamma}\vec{n} \to \pi^- p$). This proposed measurement will provide essential complimentary information to the K_{LL} measurement in experiment E12-20-008 approved by PAC48 in 2020.

As already presented in the E12-20-008 proposal, historically, theoretical calculations have underestimated – by ∼2 orders of magnitude – the observed differential cross sections measured at SLAC [1] for single pion photoproduction in the wide angle regime (where the Mandelstam variables $s, -t, -u \gg \Lambda^2_{QCD}$). Recently, theoretical developments by P. Kroll and K. Passek-Kumericki suggest a solution to this discrepancy using a GPD-based theory that includes both twist-2 and twist-3 amplitudes [2]. According to the handbag mechanism in the GPD-based framework, the signatures of the twist-3 amplitude are the cross sections and the predicted double polarization observables K_{LL} and A_{LL}, with the signs of K_{LL} and A_{LL} expected to be opposite if the twist-3 amplitude is the dominant contribution. The approved E12-20-008 experiment plans to experimentally measure the K_{LL} helicity correlation observable. The current proposal aims to measure A_{LL} at the same kinematics, therefore providing essential complementary experimental data to allow for a cross-check of the validity of the handbag mechanism in the GPD framework in the accessible energy range.

This proposed A_{LL} experiment would be performed in Hall A of Jefferson Lab and run after the approved SBS experiment E12-09-016 [31], using the same equipment. The only necessary modification will be the tracker detectors inserted in the SBS arm (already constructed for GEn-RP experiment). This additional track information will also benefit the E12-09-016 experiment for background rejection/veto purposes. The target magnetic field will be oriented along the beam by using existing configuration of the Helmholtz coils.

We plan to test three aspects of the theoretical prediction:

- Similar absolute values and opposite signs of K_{LL} and A_{LL}.
- Dependence of A_{LL} with a slight variation of the pion centre of mass angle.
- Stability of A_{LL} in the wide angle regime as a function of Mandelstam variable s in the energy range 9 to 15 GeV^2.

This experiment aims to measure helicity correlation observables that have not been measured before for wide angle pion photoproduction. **Such a pioneering measurement will help to uncover the nature of the interaction mechanism that underlies exclusive single pion photoproduction from the nucleon in the wide angle regime.**

2 Introduction

Meson photoproduction from the nucleon has been the subject of physics interest for more than 70+ years now. Many experiments were performed in 50s-60s-70s at various electron beam facilities to study exclusive photoproduction reactions. Currently, four labs are actively performing research in this field: Jefferson Lab, Bonn, Mainz, and Spring-8. Pion photoproduction from the nucleon is the simplest inelastic hadron process, so it is an important testing ground for our understanding of hadron physics.

The cross sections and other observables in the wide angle regime $(s, -t, -u >> \Lambda^2_{QCD})$ are expected to be calculable with controlled accuracy, which makes them especially useful for testing of the interaction mechanism models. Many calculations were able to predict intriguing features (such as scaling, and cross section ratios) but disagreed with the absolute cross sections. With the development of the GPDs in the last 20 years, new calculations have been performed, but the discrepancy with experiments on the absolute cross section is still too large. Only recently has a new GPD-based calculation found a possible solution for the missing cross section [2]. This experiment together with the already approved measurement of K_{LL} (E12-20-008) will provide an important test of advanced GPD-based theory.

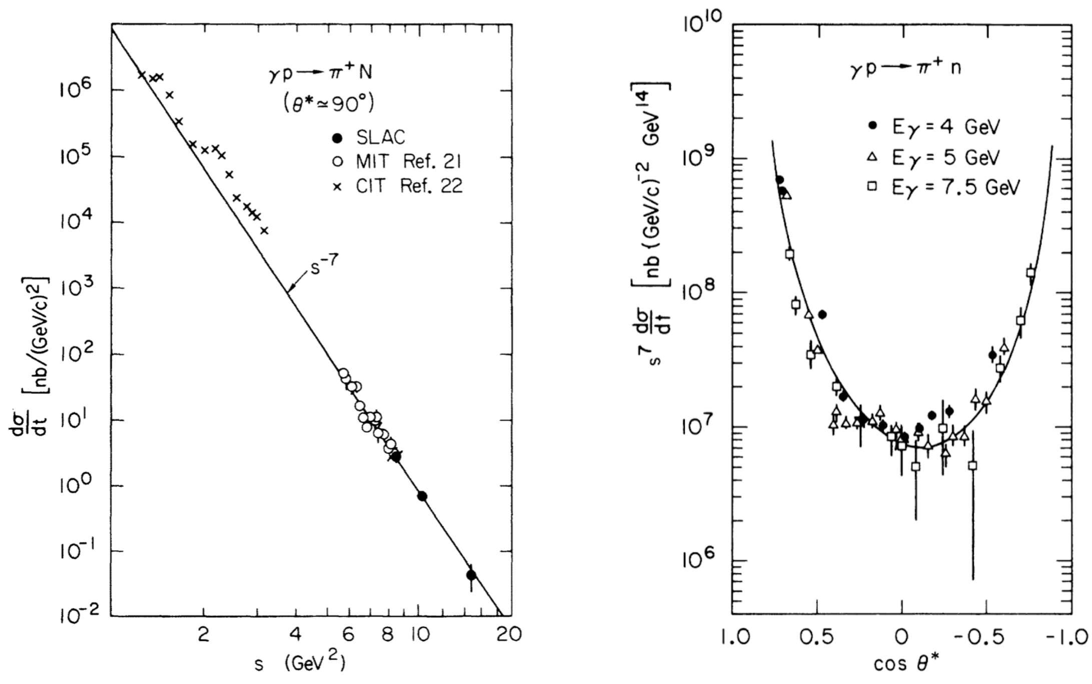

Figure 1: Left: Differential cross section $d\sigma/dt$ for the process $\gamma p \rightarrow \pi^+ N$ at 90° versus s. The solid line shows s^{-7} for reference. Right: Angular dependence of the cross section and the fit function. The figures are taken from [1].

2.1 The Field of Meson Photoproduction

The field of meson photo- and electroproduction has been an area of active research for many decades. Pioneering experiments were conducted at Stanford, where the ratios of electron-induced and photon-induced pion processes were measured at different incident beam energies in an attempt to understand the observed pion cross sections [3]. Many experiments have been performed in the resonance region since then. The cross section and all polarization observables have been investigated carefully for photon energies below 2-3 GeV, see the data base [4]. Partial-wave analyses based on these data can be found on the SAID and MAID web pages [5, 6]. The $s, -t$ and $-u$ values in those experiments are too low for applicability of currently known leading twist calculations.

For the resonance region, the Regge model of Ref. [7] was used to fit the data from SLAC and other labs. At JLab, several measurements of the cross sections of neutral and charged pions were performed for energies up to 5.5 GeV [8, 9, 10]. The linearly polarized photon asymmetry E was measured up to 2.3 GeV [10]. The polarization transfer asymmetry for the neutral pion was obtained in Refs. [11, 12] at s up to 11 (GeV/c)^2 but relatively low values of $-u$.

2.2 Scaling in Meson Photoproduction

Measurements of exclusive photoproduction processes for a variety of reactions were conducted at large values of $-t$ and $-u$ at photon energies from 4 to 7.5 GeV at SLAC [1]. Scaled cross sections as a function of $|t|$ and scattering angle θ^* were studied in detail for these reactions. For example, Fig. 1 shows the differential cross section $d\sigma/dt$ for the process $\gamma p \to \pi^+ N$ at 90° cm. angle versus s along with the s^{-7} for reference. Overall, good scaling behavior was observed at fixed center of mass angles in these measurements. At the same time, calculations missed the observed cross sections by **two orders of magnitude!**

The constituent counting rule (CCR) predicts the differential cross section at fixed center of mass angles for an exclusive two-body reaction at high energy and large momentum transfer as:

$$\frac{d\sigma}{dt} \propto \frac{f(\theta_{cm})}{s^{n-2}} \tag{1}$$

where s and t are the Mandelstam variables, θ_{cm} is the center of mass frame angle, $f(\theta_{cm})$ depends on the dynamics of the process and n is the number of active “elementary” fields in the initial and final states that are participating in the reaction. In the case of a process like $\gamma p \to \pi^+ n$, the CCR predicts an $s^{-(3+2+3+1-2)} = s^{-7}$ dependence. This model, based on dimensional analysis proposed by Gunion, Brodsky, and Blankenbecler [13], attempts to connect the observed cross section to the number of “elementary fields” participating in the reaction. Although this model is a fairly good representation of the scaling features, it falls short of explaining the absolute cross sections. A very good question, which a full theory should be able to answer, is: Why does the scaling prediction work so well?

2.3 Charged Pion Photoproduction Experiments

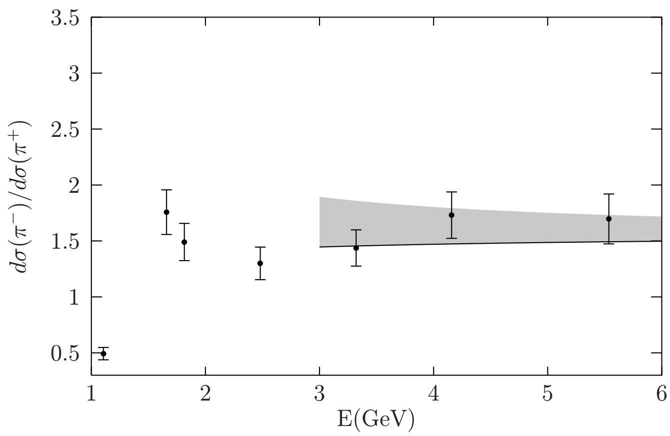

Figure 2: Ratio of differential cross sections $d\sigma(\pi^-)/d\sigma(\pi^+)$ for the process $\gamma p \to \pi^+ n$ and $\gamma n \to \pi^- p$ at 90° versus E, the energy of the incident photon. Data points are taken from [9]. The solid line corresponds to the handbag prediction, with uncertainties due to target mass corrections [15].

Differential cross section measurements of charged pions in the reactions $\gamma n \to \pi^- p$ and $\gamma p \to \pi^+ n$ were conducted in Hall A at Jefferson Lab [9]. The cross sections were measured over a wide range of photon energies from 1.1 to 5.5 GeV with pion center of mass angles ranging from $\theta_{\rm cm} = 50^\circ$ to 110°.

Several calculations done using CCR, Hadron Helicity Conservation (HHC), and the pQCD approach **fall short of the observed $\pi^\pm$ cross sections**, indicating a problem in the assumed interaction mechanism responsible for these observed cross sections. The experimental results indicate a surprising global scaling behavior at high energies and high transverse momenta, consistent with the constituent counting rule. Data also suggest an enhancement in the cross section at center of mass energies near 2.2 GeV and indicated a possible substructure around the scaling behavior.

It is important to be able to explain the observed cross sections as that sheds light on our understanding of the dynamics of interaction that operates in a particular regime. For the wide angle regime in particular, two extreme scenarios have been proposed which can be distinguished by the number of active participants in the hard scattering regime. The handbag mechanism [27, 28] involves only one active constituent, while the perturbative QCD (pQCD) mechanism involves three [13]. A depiction of the handbag mechanism is shown in Figure 3. In any given kinematic regime, quantum mechanics permits both mechanisms to contribute to the scattering amplitude. At "sufficiently high" energy the pQCD mechanism is expected to dominate, but it is not known at what s this transition takes place and how the transition to the purely pQCD mechanism emerges. Therefore, it is essential to understand

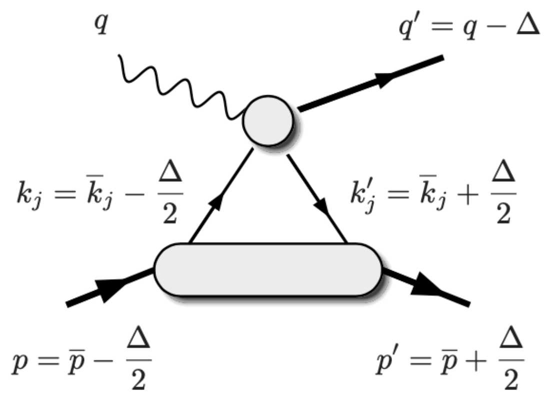

ht

Figure 3: Schematic of the handbag mechanism, which is characterized by the fact that only one quark from the incoming and one from the outgoing nucleon participate in the hard process with all others being spectators [15].

the physical mechanism that is responsible for the observed cross section in the wide angle regime.

2.4 Handbag Approach Calculations

As discussed in the the previous section, the handbag mechanism (depicted in Figure 3) is characterized by the fact that only one quark from the incoming and one from the outgoing nucleon participate in the hard process while all others become "spectators". The calculations [14] were done in order to explain the ratio of $\pi^+$and $\pi^-$for the reactions $\gamma n \to \pi^- p$ and $\gamma p \to \pi^+ n$ at large center of mass angles using the handbag approach in the framework of the GPDs. The ratio of the cross sections calculated using this approach is approximately given by

$$\frac{d\sigma(\gamma n \to \pi^- p)}{d\sigma(\gamma p \to \pi^+ n)} \approx \left(\frac{e_u s + e_d u}{e_u u + e_d s} \right)^2 \tag{2}$$

where e_u and e_d are the charges of the up and the down quarks while s and u are the Mandelstam variables. The leading order calculation for the ratio agrees quite well with experimental data for Compton Scattering suggesting that the handbag approach accurately describes the reaction for the chosen energies and angles. Recently, the cross section of π^0 exclusive photoproduction from the CLAS6 detector in Hall B of Jefferson Lab [8] (shown in Fig. 4) and calculations done by P.Kroll *et al.* [14] using a leading twist handbag model have disagreed in some kinematics, by **more than two orders of magnitude**.

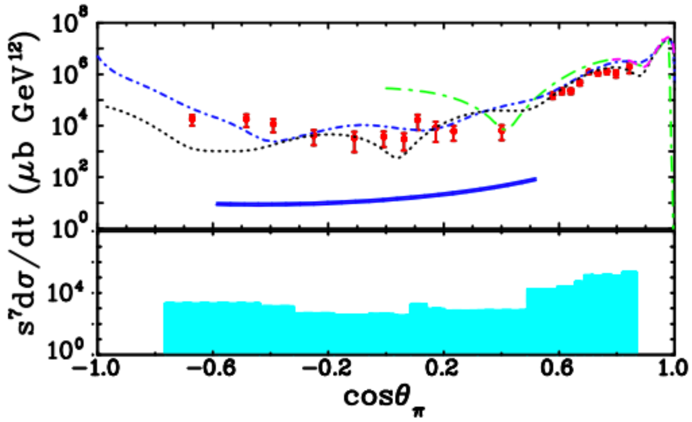

Figure 4: Differential cross section for π^0 photoproduction = new TF1 from CLAS in Hall B at Jefferson Lab. Red circles are data points from the experiment plotted along with statistical uncertainties. The systematic uncertainties are shown in the shaded blue area in the sub panel. Figure taken from [8].

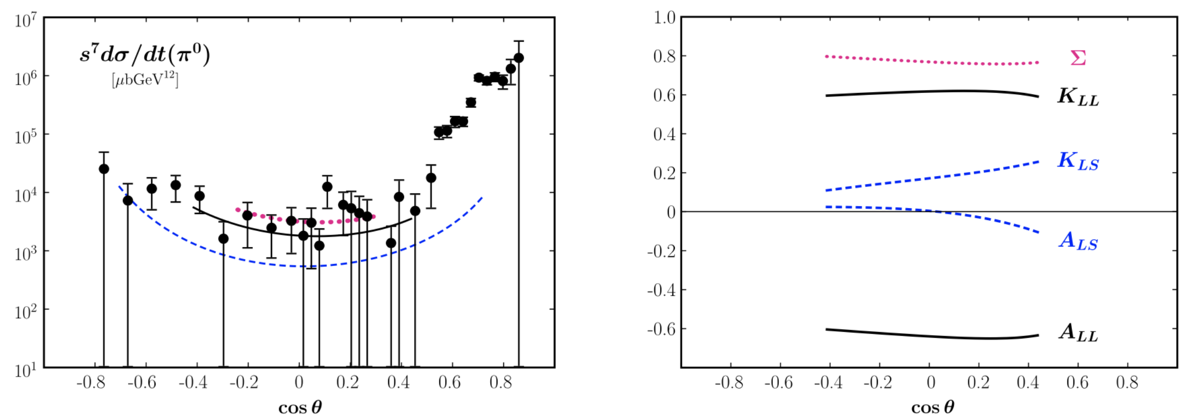

a) b)

Figure 5: a) π^0 cross section data from CLAS along with calculations made by Kroll *et al.*. Dashed, solid, and dotted lines are for s = 9, 11.06 and 20 (GeV/c)^2. b) K_{LL} and A_{LL} predictions for π^0 made by Kroll *et al.* [2].

Since leading twist calculations are unable to account for the observed π^0 cross sections, Kroll *et al.* [2] calculated the wide angle photoproduction cross section of π^0 mesons within the handbag factorization scheme. These calculations take twist-2 and twist-3 contributions into consideration in order to obtain consistent results with CLAS data [8] (shown in Figure 5-a). The twist-3 contribution dominates, while the twist-2 contribution to the cross section is almost negligible. Calculations were also performed for spin dependent observables which are the correlations between the helicities of the incoming photon (+ and -) and the longitudinal component of polarization for the initial nucleon (A_{LL}) or the final nucleon (K_{LL}). These helicity correlations are defined as follows:

$$K_{LL} = \frac{d\sigma(+,\rightarrow) - d\sigma(-,\rightarrow)}{d\sigma(+,\rightarrow) + d\sigma(-,\rightarrow)} \tag{3}$$

Similarly,

$$A_{LL} = \frac{d\sigma(+\rightarrow) - d\sigma(-\rightarrow)}{d\sigma(+\rightarrow) + d\sigma(-\rightarrow)} \tag{4}$$

where the first symbol denotes the incident photon helicity and the second denotes the proton longitudinal polarization.

$$K_{LS} = \frac{d\sigma(+,\uparrow) - d\sigma(-,\uparrow)}{d\sigma(+,\uparrow) + d\sigma(-,\uparrow)} \tag{5}$$

Similarly,

$$A_{LS} = \frac{d\sigma(+\uparrow) - d\sigma(-\uparrow)}{d\sigma(+\uparrow) + d\sigma(-\uparrow)}, \tag{6}$$

where the first symbol denotes the incident photon helicity and the second, nucleon sideways polarization, where sideways is the direction perpendicular to longitudinal in the plane of the reaction. For twist-2 contributions, the authors estimate that:

$$A_{LL}^{twist-2} = K_{LL}^{twist-2} \tag{7}$$

and for twist-3 contribution,

$$A_{LL}^{twist-3} = -K_{LL}^{twist-3} \tag{8}$$

Calculations have been made for π^0 photoproduction as shown in Figure 5 b). Similar calculations have been made for $\pi^{\pm}$ photoproduction by Kroll and Passek-Kumericki [17]. In this case, in contrast to π^0 photoproduction, the twist-2 contribution is not negligible in the forward direction whereas the twist-3 contribution dominates the backward direction. As can be seen in Fig. 6, the values of A_{LL} and K_{LL} are mostly mirror images of each other, but approach 0 for more forward angles, unlike in the π^0 case. Such helicity correlations for $\pi^{\pm}$ have not yet been measured at sufficiently large s,$-t$, and $-u$ and, as proposed, would certainly be a pioneering measurement. Such a measurement will put constraints on the contribution of twist-2 and twist-3 amplitudes to the $\pi^{\pm}$ photoproduction cross section while potentially providing empirical support for the validity of the handbag mechanism in the framework of GPDs.

In view of the experimental and theoretical advances, a resumption of the investigation of wide angle meson photoproduction is timely and necessary to complement the good agreement of the handbag mechanism with WACS case. **A test of the polarization transfer observables for Wide Angle Pion Photoproduction (WAPP) would provide valuable information on the validity of the handbag mechanism in the GPD framework in this energy range. This pioneering measurement will shed light**

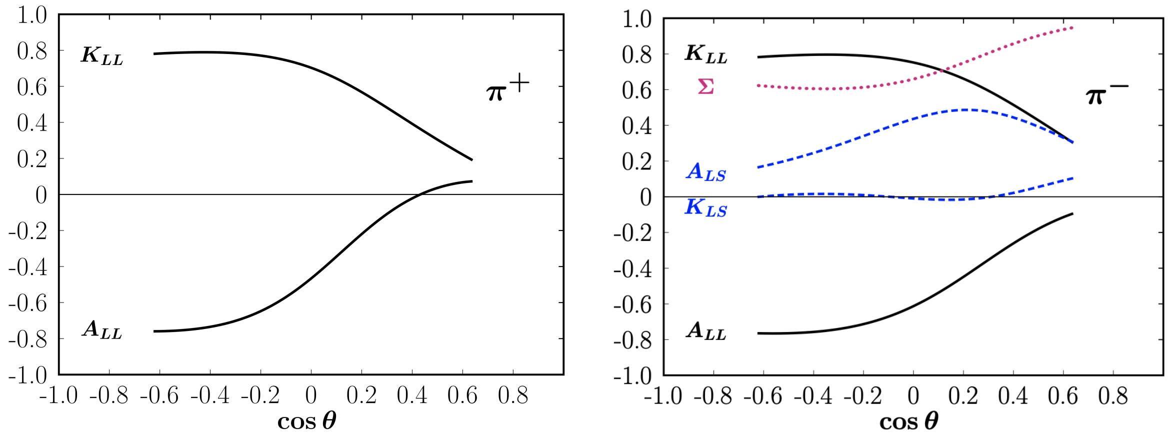

Figure 6: Predictions for helicity correlations of π^- photoproduction [2] and π^+ photoproduction [17] at $s = 15$ (GeV/c)^2. The predictions are valid only for $-t$ and $-u$ larger than 2.5 (GeV/c)^2.

on the interaction mechanism that is responsible for generating charged pions particularly in the wide angle regime.

3 Physics Motivation

The goal for the pioneering measurement of the polarization transfer observable A_{LL} for single π^- photoproduction in the wide-angle regime is to address the following questions:

- What is the nature of the interaction mechanism of meson photoproduction from the nucleon at $s, -t, -u \gg \Lambda^2_{QCD}$?
- Does the twist-3 contribution dominate the twist-2 contribution in the wide angle regime, as suggested by the updated handbag mechanism cross section calculations?

4 Experimental goals

We propose to measure A_{LL} for negatively charged pion photoproduction in the wide angle regime by using the SBS as the proton arm and BB as the pion arm. There, three aspects will be tested:

1. Does A_{LL} equal -K_{LL}?
2. Does A_{LL} have any dependence on cm. angle at $s = 9$ GeV^2 and large $-u$, $-t$?
3. Does A_{LL} have any s dependence at $s > 9$ GeV^2?

The experiment will use the 6.6, 8.8, and 11 GeV CEBAF electron beam to impinge bremsstrahlung photons on a polarized He-3 target and run with the same detector setup as the GEn/He-3 experiment (plus a front part of the SBS tracker prepared for GEn-RP (E12-17-004)). In addition to the A_{LL} measurements for the exclusive single pion process $\vec{\gamma}\vec{n} \to \pi^- p$, we expect significant statistics for the exclusive $\vec{\gamma}\vec{n} \to \pi^- \Delta^{++}$ process.

5 Experimental Setup

The experimental setup is almost identical to that of the upcoming SBS experiment E12-09-016 [31], which will measure $^{3}\overrightarrow{He}(\overrightarrow{e}, e'n)pp$. A top view of the setup for E12-09-016 in Hall A is shown in Fig 7.

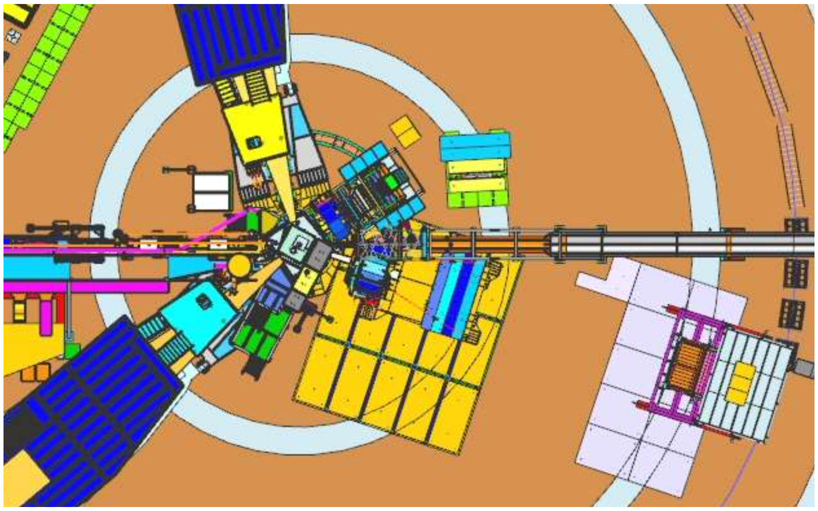

Figure 7: Top view of the E12-09-016 GEn He3 setup in Hall A. The electron beam goes from the left side.

The solid angles of the detector arms are about 50 msr with 1:4 aspect ratio (horizontal-to-vertical). Momentum acceptance of BigBite starts from 0.5 GeV/c and SBS from 1 GeV/c. These parameters allow high efficiency detection of the process with large solid angle and the missing momentum up to 200-300 MeV/c.

In E12-09-016 the recently upgraded BigBite spectrometer arm will be used for the scattered electron detection and the SBS arm (comprising the 48D48 magnet and HCAL) will be used for the neutron detection. The pion photoproduction measurement will use a similar layout to the Q^2=10 GeV^2 kinematic setting of E12-09-016, with the BigBite and SBS spectrometers positioned at 41.9 and 24.3°, respectively.

For the pion photoproduction measurement there will be some additions: insertion of a 6 % Cu radiator placed in front of the target, and the GEM tracker planes inserted before HCAL on the SBS arm. They are already prepared for use in the GEn-RP (E12-17-004) experiment during the fall 2021 data taking. Running with the radiator will require a lower beam current than originally planned for this kinematic setting in E12-09-016, to reduce background rates. We propose that the radiator be placed 10 cm upstream of the ^{3}He cell. The GEM planes will be beneficial for E12-09-016 at all of its kinematic settings, acting as VETO detectors for charged particles, and therefore we propose to leave them in SBS for the whole run period.

A summary of the experimental setup is outlined in the list below:

- CEBAF 6.6 (8.8 and 11) GeV electron beam of 20 μA current (one-third of the current compared to the same kinematic setting for E12-09-016).
- A 60 cm long and 10.5 atm $^3\overrightarrow{He}$ target as in E12-09-016, with an additional 6% radiation length Cu radiator placed 10 cm upstream of the target.
- BigBite arm to detect the π^-. It has a dipole magnet followed by GEM trackers, GRINCH (a gas Cherenkov detector), rear GEM chamber, Pb-glass preshower, timing hodoscope, and Pb-glass shower calorimeter.
- SBS arm to detect the proton. This arm has a 48D48 dipole magnet, which will be followed by five GEM chambers and a Hadron calorimeter.

5.1 The CEBAF Electron Beam

We propose to perform the measurement in Hall A of Jefferson Lab using the CW polarized 6.6 (8.8, and 11) GeV electron beam from the CEBAF accelerator. Electron beam polarizations of $\sim$ 85% have been routinely achieved, and such a beam polarization value has been assumed in the calculations of the projected statistical precision of the proposed measurement.

5.2 The BigBite spectrometer - Pion Arm

BigBite is a large-acceptance non-focusing magnetic spectrometer which subtends a solid angle of $\sim$ 50 msr when placed 1.55 m from the center of the target to the entrance of the dipole. A schematic of the BigBite arm is shown in Figure 8.

The main components of the BigBite arm are:

5.2.1 The Dipole Magnet

The 20 ton dipole magnet has been used in several experiments performed with the 6 GeV CEBAF electron beam. With the entrance aperture at 155 cm from the target center, the minimum central scattering angle that BigBite can reach is around 30°. The field integral along the central trajectory is 1.2 Tm. The angular resolutions of the detector are $\delta\theta \approx 1$ mrad for $p_\pi \approx 2.5$ GeV/c. The momentum resolution $\delta p/p \approx 1\%$ for such pion momenta. The vertex resolution is ≈ 2 mm along the direction perpendicular to the central axis of the magnet.

5.2.2 Front and Rear GEM chambers

In order to achieve higher usable luminosity, the MWPCs from the 6 GeV era of experiments have been replaced with GEM-based tracking detectors. The front GEM detector planes will be installed immediately after the dipole magnet and before the gas Cherenkov detector. For the front GEM tracker, four triple-foil GEM chambers will be installed with a total area of

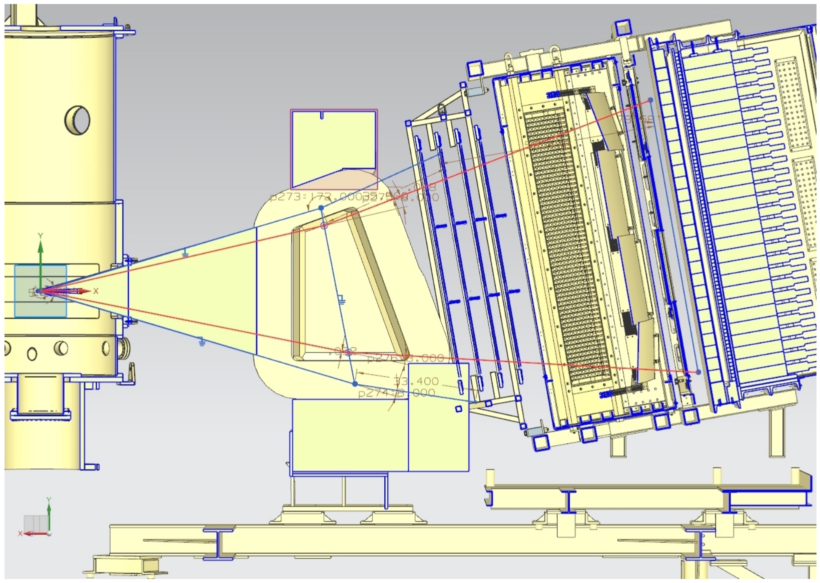

Figure 8: Schematic of the BigBite arm. See text for details.

40 cm x 150 cm. A rear GEM detector plane will be installed in between the GRINCH and the preshower calorimeter. For the rear GEM chamber, 4 GEM modules of 60 cm x 50 cm in area will be installed, giving a total area of 60 cm x 200 cm.

5.2.3 Gas Cherenkov

The gas Cherenkov detector, “GRINCH”, prepared by the College of William and Mary and collaborators, contributes greatly to off-line separation of e^- and $\pi^\pm$. Light emitted from the charged particle tracks in the detector will be reflected by four cylindrical mirrors and detected in 510 9125 PMTs which have a diameter of 29 mm. The clusters of hits in adjacent PMTs will be identified by time coincidence and location correlation with the particle trajectory.

5.2.4 Timing Hodoscope

Precision timing of a particle will be provided by the Timing Hodoscope built by a collaboration led by Glasgow University. This hodoscope consists of 90 EJ200 plastic scintillator bars, with dimensions 25 x 25 x 600 mm, each read out by ET9142 29-mm PMTs. The time resolution of 0.15 ns allows reliable identification of the individual RF buckets in the beam sent by the CEBAF accelerator. The detector will provide an accurate constraint on the vertical location of the particle track for a starting point for the track reconstruction.

5.2.5 Pb-Glass Calorimeter - Preshower and Shower

Preshower and shower components of the BigBite detector consist of lead glass blocks read out by PMTs which collect the Cherenkov light from relativistic charged particles, including the primary particles and secondary e^+/e^- produced in electromagnetic cascade events. The preshower blocks are 9 cm x 9 cm x 30 cm and have radiation hard lead-glass (reused from HERMES). The long axes of the preshower modules are oriented perpendicular to the pion direction while the long dimensions of the shower blocks are oriented along the pion direction. The energies deposited in the preshower and the shower modules will help distinguish between electrons and pions in the detector. Signals in both layers of this detector will be used in event selection for the DAQ trigger.

5.3 The Proton Arm

A schematic of the proton arm is shown in Figure 9.

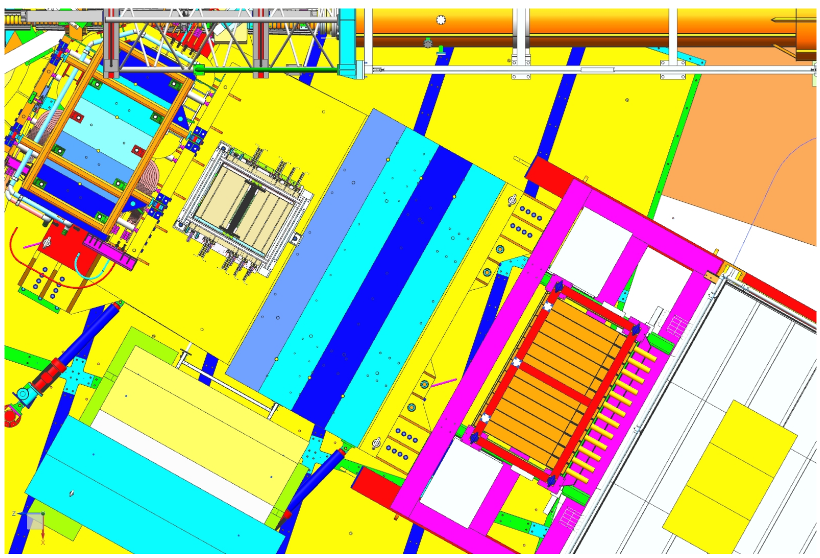

Figure 9: The schematic view of the proton arm.

The components of the proton arm are the following:

5.3.1 48D48 Dipole Magnet

The 48D48 dipole magnet (the field integral is 1.7 Tm) provides momentum analysis of the protons.

5.3.2 GEM Charged Particle Trackers

The tracker includes two GEM planes with a size of 40 cm x 150 cm (built by INFN), two similar size chambers with UV orientation of the readout strips and two bigger chambers of 60 cm x 200 cm (built by UVa). The tracker allows us to track the protons produced by interactions of the beam with the polarized He-3 target, for reconstructing the scattered proton's kinematics.

5.3.3 Hadron Calorimeter

The Hadron Calorimeter, or simply HCAL, will be used in the detection of the protons. It was built by a collaboration led by CMU and INFN/Catania with contributions from JLab and the SBS collaboration. It consists of a 12 x 24 array of 15 x 15 x 90.8 cm calorimeter modules which are formed by alternating Fe and plastic scintillator plates. The total thickness of Fe is 50.8 cm and of the plastic scintillator is 40 cm. Scintillation light will be collected by a wavelength-shifting plastic and then transmitted to a PMT. The time resolution is expected to be 0.5 ns (a combination of the time and energy information). The response to protons and neutrons will be very similar and the efficiency is expected to be $\sim 90\%$ for the protons in the proposed measurement.

5.4 The polarized He-3 target at JLab

The experiment will utilize the polarized ^{3}He target that was first constructed for E94-010 that ran in Hall A, and has subsequently been modified and upgraded for a series of experiments in both Halls A and C. In particular, we will utilize the target configuration that will be used for E12-09-016, the SBS polarized ^{3}He G_E^n experiment. Sometimes referred to as the "Stage II" polarized ^{3}He target, the design incorporates a convection-based target-cell design, making it possible to run at considerably higher luminosities. During the recent Hall C experiment to measure A_1^n, the figure of merit was typically a factor of two higher than had ever been previously achieved. The only modifications to the polarized ^{3}He target beyond the configuration that is planned for the G_E^n experiment will be those needed to accommodate the longitudinal polarization direction.

5.4.1 The technique used in the polarized He-3 target

The target is based on the technique of spin-exchange optical pumping, which in its simplest form, can be viewed as a two step process: 1) an alkali metal is polarized through optical pumping, and 2) the ^{3}He nuceli are polarized through collisions with the alkali-metal atoms through a hyperfine interaction. In fact, to increase he efficiency of the process, we use a hybrid mixture of two alkali-metal species comprising a small amount of Rb and a larger quantity of K. The Rb is optically pumped, and through collisions with the K atoms, the K becomes quickly polarized as well. Sometimes known as alkali-hybrid spin exchange optical pumping, this technique was first used during the last Hall A experiment to measure G_E^n, resulting in greatly enhanced performance of the target. Both the alkali-metal atoms and the ^{3}He are contained in a sealed glass cell.

The time-dependent polarization of the ^{3}He can be described by

$$P_{\rm He}(t) = P_{\rm Alk} \frac{\gamma_{se}}{\gamma_{se} + \Gamma} \left(1 - e^{-t(\gamma_{se}+\Gamma)}\right), \tag{9}$$

where $P_{\rm He}$ is the nuclear polarization of the ^{3}He, $P_{\rm Alk}$ is the polarization of the alkali-metal vapor, γ_{se} is the rate of spin-exchange between the ^{3}He and the alkali-metal vapor (averaged over the entire target cell), and Γ is the spin-relaxation rate of the ^{3}He nuclei due to all other processes. The spin exchange between the alkali-metal vapor and the ^{3}He is quite slow, with $1/\gamma_{se}$ being on the order of 5 hours. From equation 9, it can be seen that in order to achieve high polarizations, we must have the relaxation rate $\Gamma << \gamma_{se}$. Some of the contributions to Γ are intrinsic to the various target cells. These intrinsic contributions include relaxation due to ^{3}He–^{3}He collisions, and relaxation due to ^{3}He–wall collisions. Calling the intrinsic component to the relaxation Γ_{cell}, it is desirable to have cells in which Γ_{cell}^{-1}, which we often refer to as the cell lifetime, of ~ 25 hours or longer. Producing a collection of target cells with such long lifetimes is an important component of preparing the polarized ^{3}He target for an experiment.

5.4.2 Components of the Polarized He-3 Target

At the heart of the target system are sealed glass "target cells", shown in Fig. 10, each of which contains approximately 7.5 atmospheres of ^{3}He, around 70 Torr of nitrogen, and a few droplets of a mixture of Rb and K. The cells have two chambers: an upper "pumping chamber" in which the optical pumping and spin exchange take place, and a lower "target chamber" through which the electron beam passes during the experiment. The chambers are connected by two transfer tubes, one of which is held at a slightly higher temperature than the other one. The temperature difference of the two transfer tubes causes convective flow between the pumping and target chambers. In earlier polarized ^{3}He target cells used at JLab, only one transfer tube was used, and mixing between the two target-cell chambers occurred due to diffusion. With the convective flow, higher beam currents can be used because gas in the target chamber, that is depolarized due to ionization of the beam, is replaced more quickly. The ^{3}He is polarized in the pumping chamber, which is held at an elevated temperature of approximately 235° C using a forced hot air oven. The elevated temperature of the pumping chamber results in a ^{3}He density in the target chamber (which is much closer to ambient temperatures) of roughly 10 amagats, or the density corresponding to 10 atmospheres at STP.

The magnetic holding field is roughly 25 Gauss, and is supplied by two large sets of coils that are roughly in Helmholtz configuration. Because of the relative proximity of both the BiBite and SBS magnets, there are fringe fields that can affect the homogeneity of the magnetic field around the target. For this reason, the entire target, complete with the

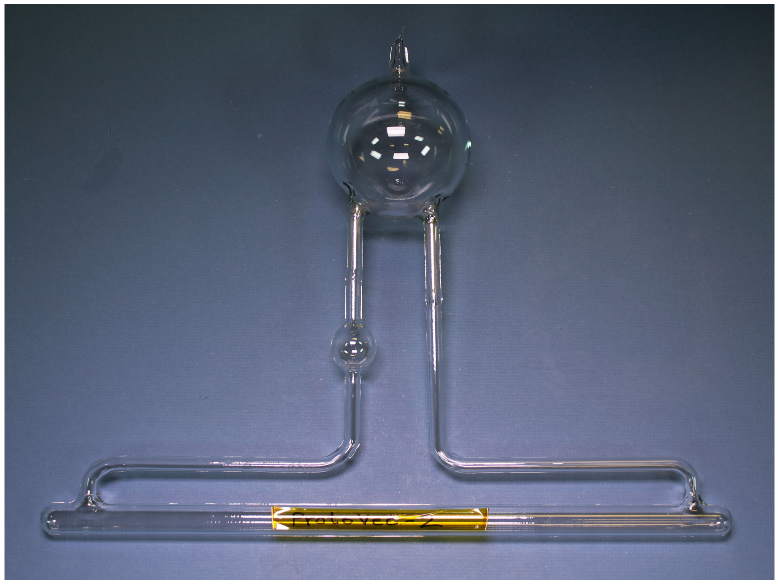

Figure 10: Shown is an example of a "convection-style" polarized ^{3}He target cell. The example shown is the geometry used during the recent Hall C A_1^n experiment which is somewhat smaller than the target cells that will be used for both the SBS G_E^n and WAPP experiments. The upper spherical portion of the cell is the pumping chamber where spin-exchange optical pumping takes place, and the lower cylindrically-shaped portion of the cell is the target chamber through which the electron beam passes.

Helmholtz coils, is enclosed in a soft iron enclosure. Extensive magnetic field studies using Tosca have shown that this arrangement is quite effective for providing the needed field.

Polarimetry is provided by two separate systems. One system is based on the NMR technique of adiabatic fast passage (AFP). During an AFP measurement, an RF field is applied to the target while the magnetic holding field is swept through the resonance condition. The resulting signal is detected by "pick-up coils". The second form of polarimetry is based on electron paramagnetic resonance (EPR). The EPR frequency of the K is measured using an optical detection scheme, and a small frequency shift is observed due to the presence of the polarized ^{3}He. The size of the shift, which is proportional to the ^{3}He polarization, can be determined in a manner that is quite free of systematics by reversing the polarization of the ^{3}He with respect to the applied magnetic field. While somewhat more time consuming than doing AFP scans, the polarimetry using EPR provides an absolute calibration of the AFP system and the level of 1-2%.

5.4.3 Pre-run Target Preparation

The following list of items will have to be performed while transitioning from GEn to the start up of the A_{LL} experiment. These pre-run changes will allow for a longitudinal polarization for a newly installed target cell after the GEn run.

- Cell and target ladder removal.
- Rotation of the magnetic field coils for a longitudinal holding field.
- Magnetic field direction measurement (to 1° accuracy).
- Reconfiguration of the optics system to accommodate the longitudinal polarization direction.
- A new ^{3}He cell installation (if needed).
- Restoration of the target ladder.

6 Proposed Measurements

The double polarization asymmetry A_{LL} in the process $\vec{\gamma}\vec{n} \to \pi^- p$ will be determined at photon energies of 4.5, 6.0, and 7.5 GeV at high $s, -t$ and $-u$, allowing for a test of the variable's sign, magnitude and kinematic dependence of the reaction mechanism on s.

6.1 Kinematics

As presented in section 4, this experiment will run with three energies of the CEBAF electron beam: 6.6, 8.8, and 11 GeV. With the 6.6 GeV beam we plan to take three kinematical points (A, B and C) as shown in table 1. Two additional data points (D and E) will be taken with higher beam energies.

	E_e GeV	θ_{π^-} deg.	E_γ GeV	p_{π^-} GeV/c	θ_p deg.	p_p GeV/c	θ_{CM} deg.	$< s >$ $(GeV/c)^2$	$< -t >$ $(GeV/c)^2$	$< -u >$ $(GeV/c)^2$
A	6.6	41.9	4.5	2.02	24.3	3.29	103	9.3	4.7	2.9
B	6.6	30.0	4.5	2.74	32.8	2.53	82	9.3	3.3	4.3
C	6.6	52.0	4.5	1.58	19.5	3.74	116	9.3	5.5	2.1
D	8.8	37.2	6.0	2.61	21.9	4.23	103	12.1	6.4	4.0
E	11	33.7	7.5	3.20	20.2	5.15	103	15.0	8.1	5.2

Table 1: Kinematic variables for five settings with 3-, 4-, and 5-pass beam.

We propose to start with the same kinematic setting as the approved WAPP-K_{LL} experiment E12-20-008, with SBS at a central angle of 24.3° and BigBite at a central angle of 41.9°. The combined acceptance of SBS and BB at these central angles is optimal for the detection of $\pi^- p$ photoproduction events at simultaneously large values of s, $-t$, and $-u$. As an example, Figure 11 shows the simulated distributions of the Mandelstam variables and the CM scattering angle θ_{CM}, for photon energies above 4 GeV for kinematic setting A. Also, Figure 12 shows the distributions of the momenta p_π and p_p of the pion and proton for kinematic setting A. The distributions shown in Fig. 11 and 12 correspond to the following requirements on the signals in the detectors:

1. Energy deposition of at least 500 MeV in the BigBite shower calorimeter
2. Energy deposition of less than 100 MeV in the BigBite preshower calorimeter
3. Energy deposition of at least 1000 MeV in HCAL (80 MeV in the scintillator material)
4. Good π^- track in the BigBite GEMs
5. Good proton track in the SBS GEMs.

In addition, the Gas Cherenkov counter will be used in off-line analysis to remove electron events and tracker will allow to remove the photon induced events.

According to calculations by Kroll et.al. [2] all of the Mandelstam variables in the proposed kinematics are sufficiently large that one might reasonably expect the handbag

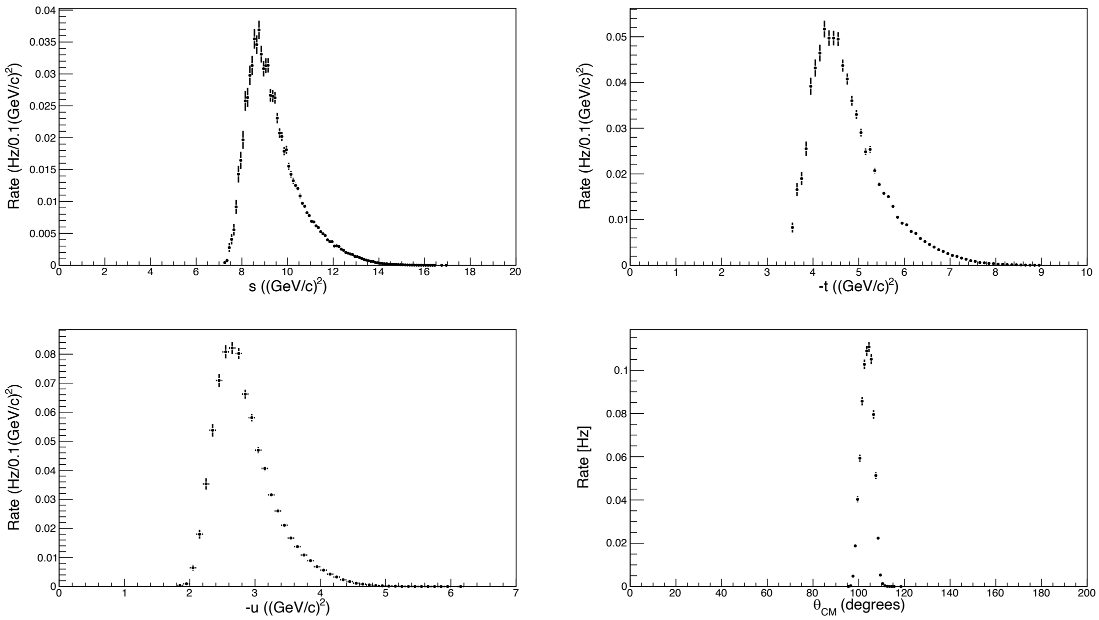

Figure 11: Distributions of s, $-t$, $-u$, and $\cos\theta_{CM}$ within the combined BigBite-SBS acceptance for kinematics A.

mechanism to play a dominant role in the observed cross sections and polarization observables.

6.2 Event Rate Analytical Calculations

The cross section of the process $\vec{\gamma}\vec{n} \to \pi^- p$ is relatively well known and parameterized as:

$$\frac{d\sigma}{dt}_{\gamma n \to \pi^- p} = 1.7 \times 0.83 \times \left(\frac{10}{s\left[\mathrm{GeV}^2\right]}\right)^7 (1-z)^{-5}(1+z)^{-4} \; \left(\mathrm{nb/GeV}^2\right), \qquad (10)$$

where $z = \cos\theta_{CM}$. The factor 1.7 was taken for the ratio of π^-/π^+ yields from a deuteron from Ref. [9], and the π^+ production cross section is from Ref. [1].

The rate of events was calculated according to the formula:

$$N_{\pi^- p} = \frac{d\sigma}{dt}_{\pi^- p} \frac{p^2_{\pi^-}}{\pi} \Delta\Omega_{\pi^-} f_{\pi^- p} \left[\frac{\Delta E_\gamma}{E_\gamma} \frac{t_{rad}}{X_o} \mathcal{L}_{en}\right] \qquad (11)$$

where $\frac{d\sigma}{dt}_{\pi^- p}$ is the process cross section; the factor $\frac{p^2_{\pi^-}}{\pi}\Delta\Omega_{\pi^-}$ is the range of Δt for the given kinematics expressed through the momentum of produced pion and the solid angle of the pion detector; $f_{\pi^- p}$ is the fraction of events detected in the proton arm for a given range of photon energy E_γ; $\frac{\Delta E_\gamma}{E_\gamma}\frac{t^{eff.}_{rad}}{X_o}$ is the number of photons per incident electron in the photon energy range $\frac{\Delta E_\gamma}{E_\gamma}$ with the radiator thickness $t^{eff.}_{rad}$ which includes the photons produced

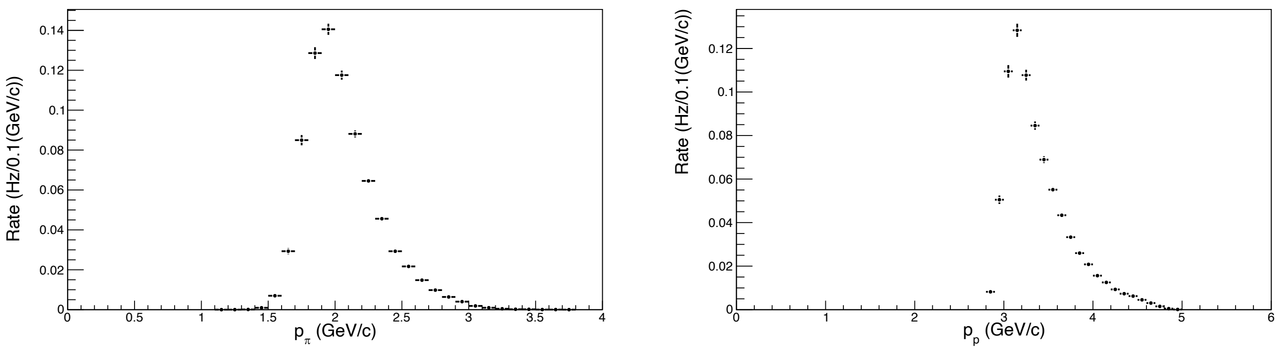

Figure 12: Distributions of p_π momentum in BigBite, and p_p momentum in SBS for kinematics A.

in the target and quasi-real photons; and $\mathcal{L}_{e-n}$ is the electron-neutron luminosity for a projected beam current. The factor $f_{\pi^- p}$ was estimated using Jacobian coefficients for each kinematics and accurately calculated using MC code. The value of $\frac{\Delta E_\gamma}{E_\gamma}$ obtained from the s distribution is about 0.15. With 6% radiator the value of $t_{rad}^{eff.}/X_o = 0.082$. The polarized electron-neutron luminosity $\mathcal{L}_{en} \sim 1.8 \times 10^{36}\text{cm}^{-2}\text{s}^{-1}$. The BigBite solid angle Ω_{π^-} is taken as 50 msr for our calculations. The factor $f_{\pi^- p}$ obtained from simulations and the statistics (without efficiency corrections) per hour are presented in table 2.

Kinematics	A	B	C	D	E
Factor $f_{\pi^- p}$	0.31	0.18	0.51	0.35	0.37
Statistics (per hour)	6000	4600	5300	2100	510

Table 2: Estimated statistics of $\pi^- p$ events in each kinematics per one hour of running.

6.3 Additional Statistics Reduction Factors

The event rate shown in table 2 needs to be corrected for detection efficiencies of the pion and proton triggers, the DAQ dead time (20%), and the requirement on $|p_{miss,\perp}|$ to be below 0.1 GeV/c, where $|p_{miss,\perp}|$ is the perpendicular component of the missing momentum. Estimated statistics of $\pi^- p$ events in each kinematics per one hour of running after applying pion and proton detection efficiencies, $|p_{miss,\perp}|$ are presented in table 3.

Kinematics	A	B	C	D	E
Pion detection efficiency	0.41	0.38	0.37	0.42	0.37
Proton detection efficiency	0.86	0.81	0.88	0.92	0.93
High $p_{miss,\perp}$ cut loss	0.85	0.86	0.82	0.82	0.84
Rate of good events per hour	1420	980	1150	530	120

Table 3: Statistics reduction factors and the final rate of good $\pi^- p$ events for each kinematics for one hour of running.

6.4 Trigger and Estimated Rates

In this section we discuss the trigger rates in the two spectrometers. It defines the DAQ trigger rate. DAQ projected dead time is about 20% at a trigger rate of 5 kHz.

6.4.1 BigBite Charged Pion Trigger

The majority of particles at the BigBite shower detector are $\pi^\pm$ and photons (from π^0 decay). The fraction of electron rate is below 5% for the particles with energy above 300 MeV and scattering angles above 30 degrees, see Fig. 13. The rates in Fig. 13 were calculated using GEANT-based DINREG MC code [36] with an electron beam on a 1 mm carbon target (0.26 g/cm^2). In this experiment the full electron-nucleon luminosity per incident electron is half as much in DINREG MC calculations. But the pions and photon rates triple due to the radiator on the beam line (according to our empirical observation). The resulting prediction for the trigger rate in BigBite is $\sim$ 500 kHz at 500 MeV threshold, which is close to the value obtained using the prediction with the PYTHIA generator used in the proposal for E12-20-008.

The standard BigBite trigger is designed to be highly efficient for electrons while suppressing charged pions and low energy particles. To facilitate this, a trigger was developed for the approved E12-20-008 experiment which focuses on optimizing charged pion detection. The design of such a trigger benefits from the structure of the BB shower detector which has two layers allowing use of a difference in the longitudinal profiles for the pion and photon/electron induced showers. By using two layers of the shower detector in the trigger, the tracker, and the Gas Cherenkov in off-line analysis, we can select π^- events with very small contamination.

We plan to use the BigBite trigger, which requires an energy deposit in the shower greater than 500 MeV and reject events if the signal in the preshower is larger than 100 MeV. Such a logic allows $\sim$40% efficiency to detect charge pions while reducing the BigBite trigger rate to an acceptable 400 kHz (combined rate of pions, photons and electrons with the proposed trigger logic).

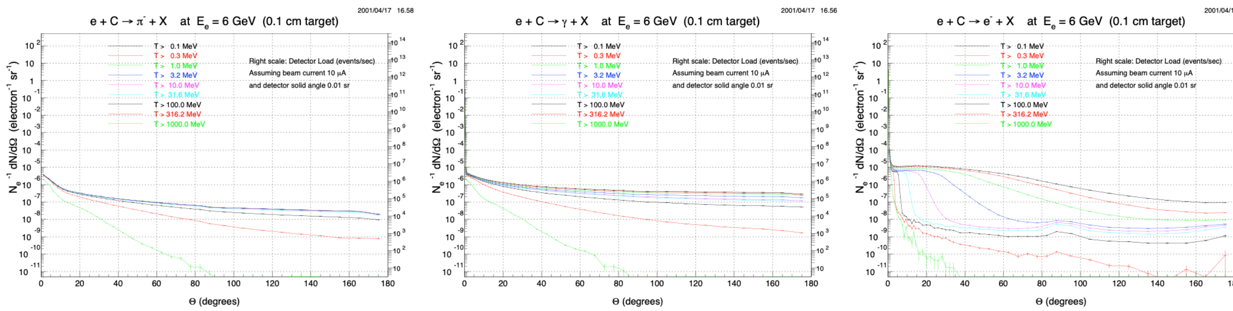

Figure 13: MC predictions for the particle rates (note the target thickness).

6.4.2 HCAL Trigger

The proton arm trigger is provided by the HCAL detector. Several MC calculations have been performed for HCAL. They found that for nucleons with energy 2 GeV and higher the detection efficiency of HCAL is close to 90% with a threshold of 80 MeV energy deposition in the calorimeter scintillator material, see Figure 14.

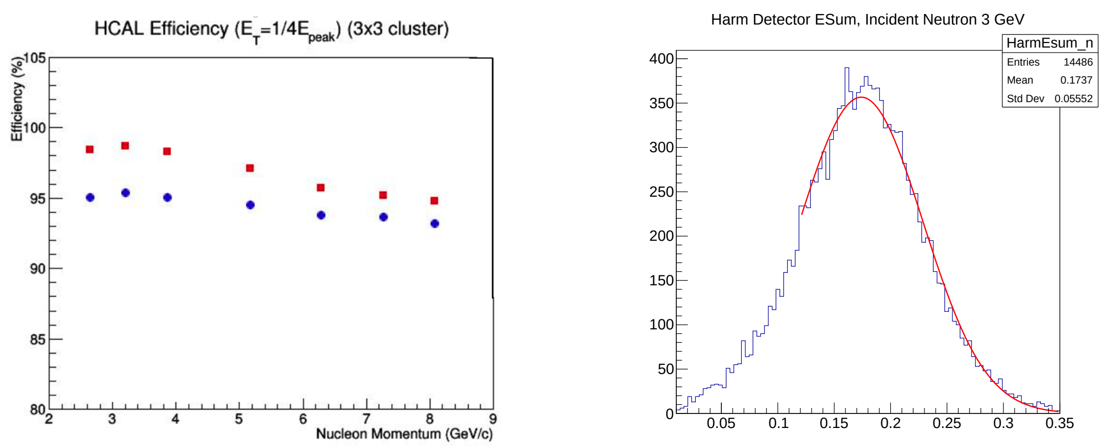

Figure 14: Left: HCAL efficiency as a function of the nucleon momentum. Right: The amplitude spectra for a 3 GeV incident neutron (scale in GeV).

The HCAL trigger rate simulation is shown in Figure 15. For the 80 MeV threshold the estimated rate is 400 kHz, which is also consistent with the DINREG calculation shown in Figure 13.

6.4.3 DAQ Trigger Rate Estimates

We plan to use a coincidence time window of 30 ns for signals from BigBite and HCAL. With 400 kHz in each arm this leads to an accidental rate of 4.8 kHz.

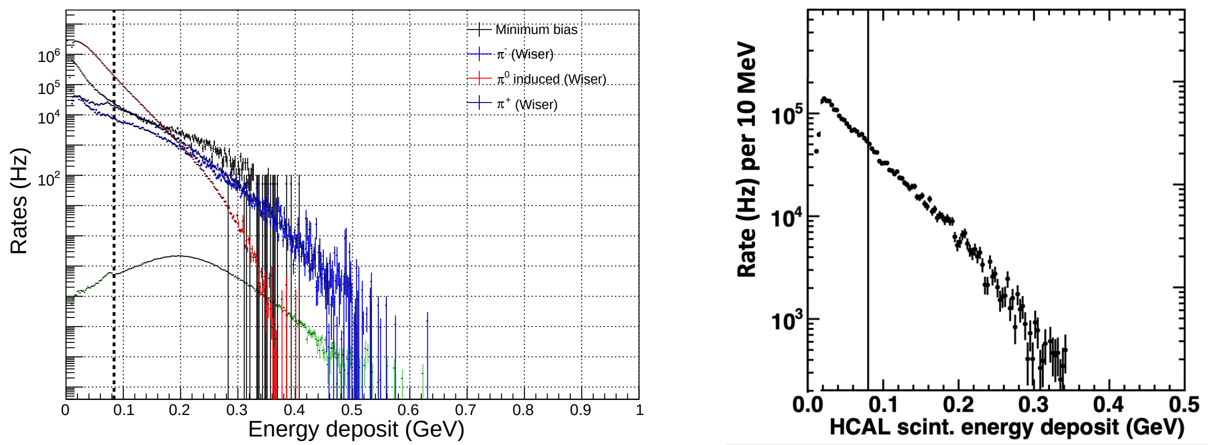

Figure 15: HCAL rate vs. energy deposition. Left: Rate above the given threshold (figures is taken from E12-20-010). Right: Rate per 10 MeV (figure is taken from E12-20-008). Figures are corrected to the luminosity of this proposal.

7 Exclusive Event Selection

In the proposed experiment, the trajectory of both final state particles will be reconstructed with angular accuracy of a few milli radians and momentum resolution of about 1%. Offline analysis allows selection of the exclusive $\gamma n \to \pi^- p$ process by using two distinct features of the photon induced exclusive reaction with two-body final state:

- The sum of the pion and proton momentum component which is transverse to the beam direction is equal to the transverse component of the neutron momentum in ^{3}He (ignoring tiny transverse momentum of the photon).
- The sum of the pion and proton energies is equal to the sum of the incident photon energy and the mass of the neutron (ignoring off-shell correction).

The coplanarity between the π^- and p production planes will also be used to isolate exclusive events. The resolution in this parameter is limited primarily by the momentum of a neutron in the ^{3}He nucleus. The total momentum of the pion and proton, $\vec{p}_{\pi^-}+\vec{p}_p$, projected to the plane perpendicular to the beam direction is the missing perpendicular momentum, $\vec{p}_{miss,\perp} = \vec{p}_{\pi,\perp} + \vec{p}_{p,\perp}$. The component of $\vec{p}_{miss,\perp}$ normal to the proton (or pion) production plane, $\vec{p}_{miss,\perp,acomp}$, provides a measure of the event "acoplanarity", which could also be characterized by the angle between the pion production plane and the proton production plane. Figure 16 shows the distributions of the absolute value of $p_{miss,\perp}$ which will be used to remove inelastic and other non-exclusive events by a cut: $p_{miss,\perp} \leq 0.1$ GeV/c. An even more effective cut is on $\vec{p}_{miss,\perp,acomp}$. These distributions include the effects of Fermi motion (dominant effect) and spectrometers resolution.

The incident photon energy E_γ in the case of the $\vec{\gamma}\vec{n} \to \pi^- p$ process is equal to E_{π^-} +

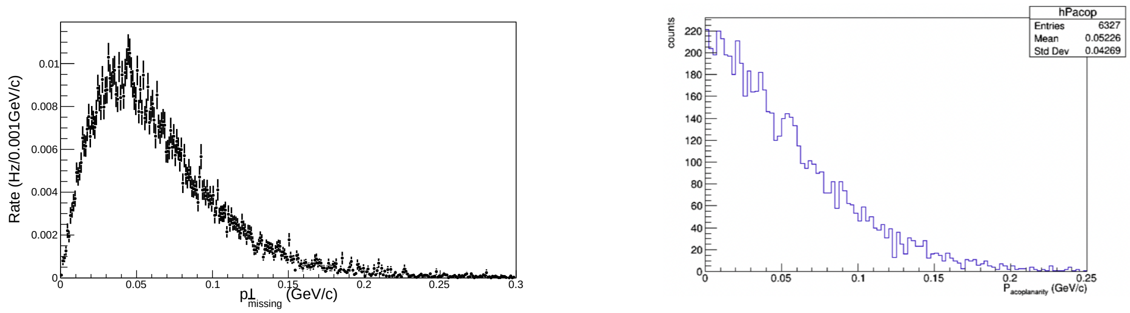

Figure 16: Missing perpendicular momentum distribution (Left) and its acoplanarity component (Right).

$E_p - m_n$. It also could be calculated using Eq. 12 as:

$$E_\gamma = \frac{s_{p\pi} - m_n^2}{2(E_\pi + E_p - p_\pi \cos\theta_\pi - p_p \cos\theta_p)} \tag{12}$$

$$s_{p\pi} = (E_p + E_\pi)^2 - (\mathbf{p}_p + \mathbf{p}_\pi)^2 \tag{13}$$

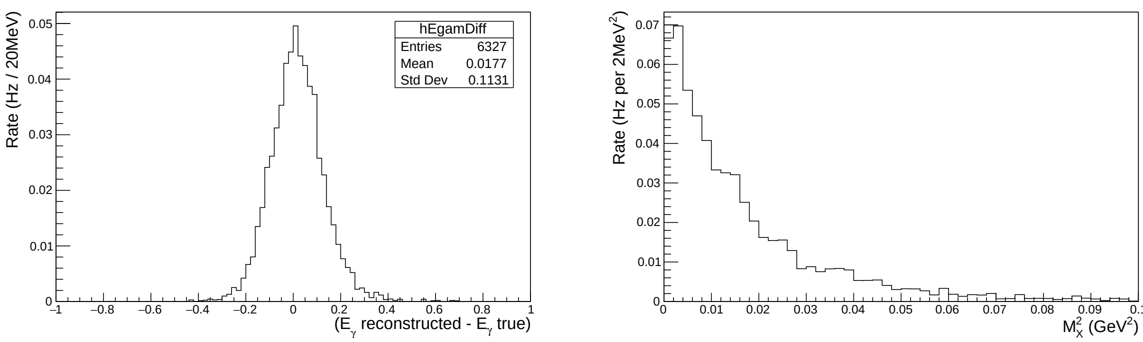

Figure 17: Left: The reconstructed photon energy minus a true photon energy (in MC). Right: Distribution on the missing mass square.

The E_γ will be reconstructed with an accuracy of 100 MeV (see Figure 17-left), which allows us to remove almost all background of events with two or more missing pions. Additionally, the missing mass parameter $M_X^2 = \left(P_\gamma^\mu + P_n^\mu + P_{\pi^-}^\mu + P_p^\mu\right)^2 \leq 0.05$ GeV^2 will be used to remove such background (Figure 17-right).

7.1 Two-pion background

The photo-production processes with two pions in the final state present significant background. The missing perpendicular momentum is the effective parameter which can be used to suppress such non-exclusive events. The missing mass parameter does not have the accuracy needed for suppression of events with one pion missing but is productive in the case of multi pion events.

Among all two-pion final state channels the events due to the reaction $\gamma p \to \pi^- \Delta^{++}$ are the most difficult to eliminate because of a relatively low momentum ($\sim$ 200 MeV/c) of the π^+ in Δ^{++} decay. The cross section for $\gamma p \to \pi^- \Delta^{++}$ process was measured at Bonn [32] for the photon energies up to 2.5 GeV and at SLAC [1, 34] for the photon energy from 5 up to 16 GeV (see Figure 18).

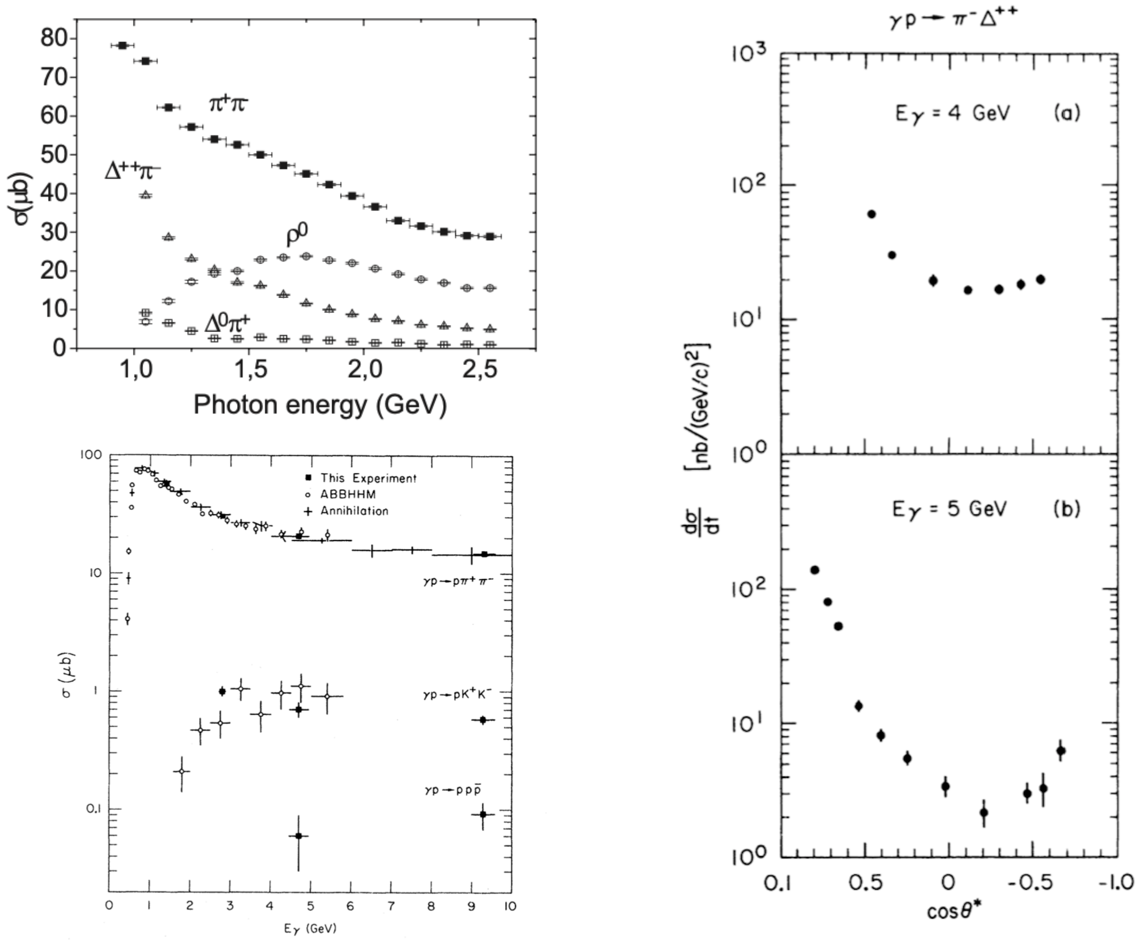

Figure 18: Cross section of Δ^{++} production. Figures are taken from Refs. [1, 32, 35].

We used data from the SLAC and JLab measurements to estimate the cross section for kinematics in our experiment. The ratio $d\sigma/dt_{(\pi^- \Delta^{++})}$ to $d\sigma/dt_{(\pi^- p)}$ is ~ 1.4 at the parameters of the kinematics A. After selection of events with $p_{miss,\perp} < 0.1$ GeV/c, contribution of this background is reduced by a factor of 4-5. The remaining background is sufficiently small and its contribution to A_{LL} could be taken into account by using data with high $p_{miss,\perp}$. The dilution of the A_{LL} asymmetry affects the statistical accuracy and should be taken into account in calculation of the required statistics.

8 Detector Calibrations

In order for us to accurately determine the produced pion direction, momentum, and the position of the production vertex along the target, the optics of BigBite need to be checked. The following calibration runs for each kinematic setting are essential to accomplish these needs:

- Data from a multi-foil carbon target and a removable lead sieve located at the front face of the BigBite magnet provide an accurate method to calibrate the angular coordinates before magnetic deflection and a beamline scattering vertex position.

- Data from elastic electron scattering from hydrogen in the reference cell will calibrate the BigBite momentum which will be performed for the 6.6 GeV beam energy setting.

- Data on an empty reference cell will have to be taken which will be used for background subtraction from the glass cell walls.

As discussed in section 6.4, the BigBite spectrometer trigger in the GEn experiment is optimized for detecting electrons. Additional beam time is needed at the beginning of the experiment to perform a trigger checkout under beam conditions.

9 Beam Time Request and Expected Results

We propose an experiment to measure the helicity correlation parameter, A_{LL} for meson photo-production in the wide angle regime for five different kinematic settings. This proposed experiment will be performed in Hall A of Jefferson Lab using the SBS apparatus, a 60 cm long polarized ^{3}He target, a 6% copper radiator and three different CEBAF beam energies at 20 μA beam current.

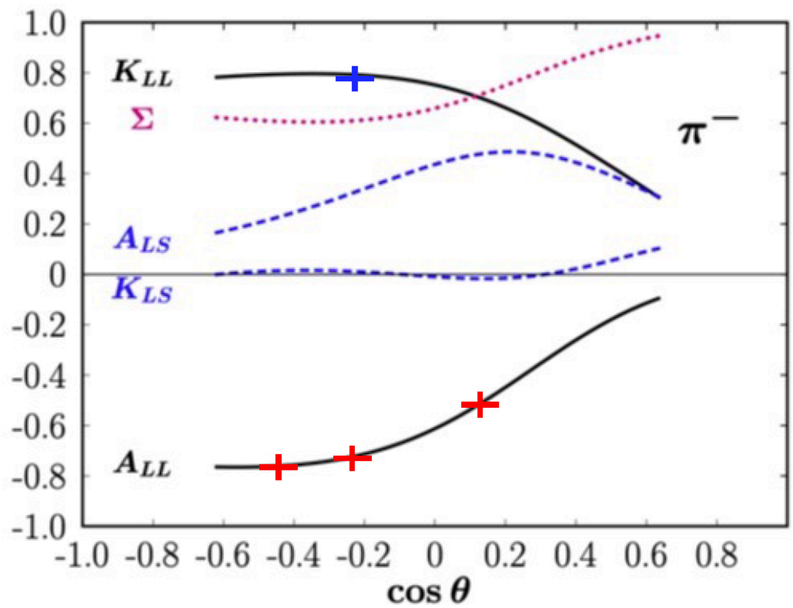

Figure 19: Projected results of this experiment for A_{LL} (shown as red) as well as projected K_{LL} data point from approved E12-20-008 (shown as blue).

The total beam time includes the following items: the production at five kinematics (96 hours, which takes into account the photon polarization, neutron polarization, and dilution due to remaining $\pi^-\Delta^{++}$ events), four times two spectrometers angle change (16 x 4 = 64 hours), target polarization measurement every 4 hours (0.25 x (96/4) = 6 hours), one measurement of the beam polarization (12 hours), BigBite spectrometer trajectory vertex data with a multi-foil target for each kinematics (2 x 5 = 10 hours), three beam energy changes with tuning of the beam position at the target (12 x 3 = 36 hours), trigger checkout for pions detection in BigBite (4 hours). **The full requested beam time is 236 hours or ∼10 days.** The projected result for A_{LL} is shown in Fig. 19. Parameters of the measurement are summarized in Tab. 4.

E_γ	$< s >$	$< -t >$	$< -u >$	$\cos\theta_{CM}$	Beam on	Time	ΔA_{LL}
[GeV]	[(GeV/c)^2]	[(GeV/c)^2]	[(GeV/c)^2]		target [hour]	[hour]	accuracy
4.0-5.5	9.3	4.7	2.9	-0.23	6	37	±0.05
4.0-5.5	9.3	3.3	4.3	+0.14	8	27	±0.05
4.0-5.5	9.3	5.5	2.1	-0.44	8	27	±0.05
5.0-7.5	12.1	6.4	4.0	-0.23	16	47	±0.05
6.5-9.0	15.0	8.1	5.2	-0.23	60	98	±0.05

Table 4: Parameters of the proposed experiment on polarization asymmetry in process $\vec{\gamma}\vec{n} \to \pi^- p$.

10 Summary

We propose to measure double spin asymmetry A_{LL} for charged pion photoproduction in the wide angle regime for the reaction ($\vec{\gamma}\vec{n} \to \pi^- p$). This proposed measurement will provide essential complimentary information to the K_{LL} measurement in an experiment E12-20-008 approved by PAC48 in 2020. The wide angle charged pion photoproduction is considered a challenging and productive test of calculations of cross sections from first principles. Several calculations fall short of explaining the observed cross sections indicating a lack of understanding of the nature of the interaction mechanism, particularly for the wide angle regime. Only recently do calculations based on the handbag mechanism in the framework of the GPDs agree with the observed cross sections. Hence, a test of the helicity correlation observables, K_{LL} and A_{LL} in high $s, -t$ and $-u$ regime is timely and necessary to verify the validity of this approach.

This measurement of A_{LL} will be the first of its kind and complementary to the K_{LL} which has been incorporated into the GMn run plan scheduled to take place during fall 2021. **Proposed is a pioneering measurement which will help establish the nature of the interaction mechanism that is responsible for the exclusive single pion photoproduction from a nucleon in the wide angle regime.**

References

[1] R.L. Anderson *et al.*, *Phys. Rev.* **D 14**, 679 (1976)

[2] P. Kroll, K. Passek-Kumericki, *Phys. Rev.* **D 97**, 074023 (2018)

[3] W. K. H. Panofsky and W. M . Woodward, and G. B. Yodh, *Phys. Rev.* **102**, 1392 (1956)

[4] The Durham HEP Reaction Data Databases (UK) (Durham HepData): `http://durpdg.dur.ac.uk/hepdata/reac.html`

[5] Partial-Wave Analyses at GW, `http://gwdac.phys.gwu.edu`

[6] Photo- and Electroproduction of Pions, Eta, Etaprime and Kaons on the Nucleon, `https://maid.kph.uni-mainz.de`.

[7] M. Guidal, J.-M. Laget and M. Vanderhaeghen, Nucl. Phys. A 627 (1997) 645; J.M. Laget, Phys. Lett. B 685 (2010) 146; J.M. Laget, Prog.Part.Nucl.Phys. 111 (2020) 103737

[8] M.C. Kunkel *et al.*, *Phys. Rev. C* **98**, 015207 (2018)

[9] L.Y. Zhu *et al.*, *Phys. Rev. Lett.* 91 (2003) 022003; Phys.Rev. C71 (2005) 044603

[10] D. Ho *et al.*, *Phys. Rev.* **C 98**, 045205 (2018)

[11] C. Fanelli *et al.*, *Phys. Rev. Lett.* **115**, 152001 (2015)

[12] W. Luo *et al.*, *Phys. Rev. Lett.* 108 (2012) 222004

[13] J.F. Gunion, S.J. Brodsky, R. Blankenbecler, Phys. Rev. B **39** 649 (1972); S.J. Brodsky and G. Farrar, *Phys. Rev. Lett.* **31**, 1953 (1973); V. Matveev *et al.*, *Nuovo Cimento Lett.* **7**, 719 (1973); S. J. Brodsky and G. P. Lepage in *Perturbative Quantum Chromodynamics*, edited by A. Mueller (World Scientific, Singapore, 1989); S. J. Brodsky and G. P. Lepage, *Phys. Rev.* **D 22**, 2157 (1980)

[14] H.W. Huang, R. Jakob, P. Kroll, K. Passek-Kumericki, *Eur. Phys. J.* **C 33**, 91 - 103 (2004)

[15] H.W. Huang, P. Kroll, T. Morii, *Eur. Phys. J.* **C 23**, 301 (2002).

[16] H. W. Huang, P. Kroll, *Eur. Phys. J.* **C 17**, 423-425 (2000).

[17] P. Kroll, K. Passek-Kumericki, private communication (2019)

[18] M. Diehl and P. Kroll, Eur.Phys.J. C73, 2397 (2013)

[19] D.J. Hamilton, V.H. Mamyan *et al.*, *Phys. Rev. Lett.* **94**, 242001 (2005)

[20] A. Danagoulian, V.H. Mamyan *et al.*, *Phys. Rev. Lett.* **98**, 152001 (2007)

[21] P. Kroll, arXiv:1703.05000

[22] M. Diehl *et al.*, *Phys. Rev.* **D 67**, 037502 (2003).

[23] F. Cano and J.M. Laget, Phys. Lett. B 551, 317 (2003)

[24] T. Brooks and L. Dixon, *Phys. Rev.* **D 62** 114021 (2000)

[25] G.A. Miller, *Phys. Rev.* **C 69**, 052201(R) (2004)

[26] B. Sawatzky, V. Bellini, K. Gnanvo, D. Hamilton, M. Kohl, N. Piskunov, and B. Wojtsekhowski, spokespersons, JLab experiment E12-17-004.

[27] X. Ji, *Phys. Rev.* **D 55**, 7114 (1997), *Phys. Rev. Lett.* **78**, 610 (1997)

[28] A.V. Radyushkin, *Phys. Lett.* **B 380**, 417 (1996), *Phys. Rev.* **D 56**, 5524 (1997)

[29] S. N. Basilev *et al.*, Eur. Phys. Journal A **56**, 26 (2020)

[30] A. J. R. Puckett *et al.*, Phys.Rev.C **96** (2017) 5, 055203, Phys.Rev.C **98** (2018) 1, 019907 (erratum)

[31] G. Cates, S. Riordan, and B. Wojtsekhowski, spokespersons, JLab experiment E12-09-016.

[32] B. H. Schoch, Eur. Phys. Journal A **19S1**, 257 (2004)

[33] A. M. Boyarski *et al.*, *Phys. Rev. Lett.* **21**, 1767 (1968)

[34] A. M. Boyarski *et al.*, *Phys. Rev. Lett.* **22**, 148 (1969)

[35] H. H. Bingham *et al.*, *Phys. Rev.* **D 8**, 1277 (1973)

[36] P.V. Degtyarenko, M.V. Kossov, H-P. Wellisch, Chiral Invariant Phase Space Event Generator, *Eur. Phys. J.* **A 8**, p. 217 (2000).